Physics of Fluids ARTICLE scitation.org/journal/phf

# Modeling of gas transport in porous medium: Stochastic simulation of the Knudsen gas and a kinetic model with homogeneous scatterer

Cite as: Phys. Fluids 32, 102004 (2020); doi: 10.1063/5.0024636
Submitted: 10 August 2020 • Accepted: 15 September 2020 •
Published Online: 5 October 2020



Shigeru Takata,[a),b)] Kisho Hatakenaka, Masanari Hattori,[a),c)] and Fumiyoshi Kasahara

## AFFILIATIONS

Department of Aeronautics and Astronautics, Graduate School of Engineering, Kyoto University, Kyoto 615-8540, Japan

**Note:** This paper is part of the Special Topic, Advances in Micro/Nano Fluid Flows: In Memory of Prof. Jason Reese.
[a)] **Also at:** Research Project of Fluid Science and Engineering, Advanced Engineering Research Center, Kyoto University, Kyoto 615-8540, Japan.
[b)] **Author to whom correspondence should be addressed:** takata.shigeru.4a@kyoto-u.ac.jp
[c)] **Electronic mail:** hattori.masanari.4r@kyoto-u.ac.jp

## ABSTRACT

Mass transport of the Knudsen gas in a porous medium is investigated on the basis of the kinetic theory of gases. First, the mass flow conductance is computed numerically for various porosities and solid grain sizes by stochastic particle simulations (SPS). Then, a kinetic model with a homogeneous scatterer is introduced, which contains the reference Knudsen number as the sole parameter that characterizes the collision frequency of gas molecules with the micro-structural solid surface. With the aid of the standard asymptotic analyses for small and large Knudsen numbers combined with the percolation theory, the effective reference Knudsen number is identified to reproduce the SPS results for a wide range of porosities.



## I. INTRODUCTION

Mass transport of fluids in a porous medium has been attracting interest of researchers in various fields, e.g., mining oil and shale gas, membrane separation, and fuel cell technologies. The porous medium has also been used in recent experimental works on thermally driven pumps and their variants.[1] The related fields are vast, and getting acquainted with every detail is difficult to achieve. Our present interest is limited to the gas transport in a porous medium.

It is widely accepted that the gas transport in a porous medium is well predicted by the framework of the conventional fluid dynamics (FD), as far as the pore size is moderate. However, as the pore size decreases typically down to the micrometer scale, it ceases to work well due to the breakdown of the continuum mechanical assumption underlying the conventional FD. Indeed, gas transport is known to show a different feature from the liquid transport, which is called the Klinkenberg effect. The Klinkenberg effect is often explained as the occurrence of slip over the micro-structural solid surface. The modification of the coefficient in the Darcy law under this interpretation implies the slip-flow correction to the conventional FD and thus naturally falls into the correction in the regime where the gas kinetic effect appears only weakly. Some recent works are motivated to extend the reliable modification toward the transition regime where the kinetic effect is not small enough to apply the slip-flow correction (see, e.g., Refs. 2–6 and the references therein). In the present paper, we are going to consider the situation where the gas kinetic effect is maximized, namely, the so-called Knudsen gas regime where molecular collisions with the solid microstructure are dominant, compared to the intermolecular (gas–gas) collisions.

More specifically, we consider a gap filled with a porous medium that separates two huge gas reservoirs and study the gas

transport numerically by stochastic particle simulations (SPS) for various solid and pore configurations inside the medium. Then, we introduce a simple kinetic model with a homogeneous scatterer. The model is simple and has a single parameter (the reference Knudsen number) that characterizes the frequency of the molecular collisions with solid. We shall establish an effective method of reproducing the stochastic simulation results by the homogeneous-scatterer model (HSM) for a wide range of volume fractions of the solid with the aid of the percolation theory.[7–11]

## II. PROBLEM AND FORMULATION

Consider a porous medium that occupies the band area between $X_1 = \pm L$, where $X_i$ are the rectangular coordinates ($i = 1$, 2, and 3). The medium is kept at a uniform temperature $T_0$ and separates the bulk gas into two regions $X_1 < -L$ and $X_1 > L$. In the former, the gas is in the equilibrium state at rest with pressure $p^-$ and temperature $T_0$, while in the latter, it is in a different equilibrium state at rest with pressure $p^+$ and temperature $T_0$ (see Fig. 1). We shall investigate the gas transport between the separated gas regions through the medium under the following assumptions:

1. the gas behavior is described by the collisionless Boltzmann equation for a monatomic perfect (ideal) gas;
2. the velocity distribution function (VDF) of gas molecules reflected on the surface of the solid is the half-Maxwellian characterized by the surface temperature and velocity (the diffuse reflection[12]);
3. the state of the gas is periodic in the $X_2$- and the $X_3$-direction with period $2L$; and
4. the temperature and the (microscopic) geometry of the solid part of the porous material do not change in time.

### A. Formulation and reduction of problem

Let us denote by $\boldsymbol{\xi}$ the molecular velocity, by $f(\boldsymbol{X}, \boldsymbol{\xi})$ the velocity distribution function of gas molecules, and by $R$ the specific gas constant. Then, taking into account the periodic assumption in the $X_2$- and the $X_3$-direction, the steady behavior of the gas in the concerned gap is described by the following boundary-value problem for $f$:[12,13]

$$\xi_i \frac{\partial f}{\partial X_i} = 0, \quad \boldsymbol{X} \in \Omega_g,$$

$$f(X_1, X_2, X_3) = f(X_1, X_2 + 2L, X_3),$$

$$f(X_1, X_2, X_3) = f(X_1, X_2, X_3 + 2L),$$

$$f\big|_{X \in \partial\Omega_s} = \left(\sqrt{\frac{2\pi}{RT_0}} \int_{\xi \cdot n < 0} |\boldsymbol{\xi} \cdot \boldsymbol{n}| f d\boldsymbol{\xi}\right) M_0, \ \boldsymbol{\xi} \cdot \boldsymbol{n} > 0,$$

$$f\big|_{X_1 = \pm L} = (p^{\pm}/RT_0) M_0, \quad \xi_1 \lessgtr 0,$$

where

$$M_0 = \frac{1}{(2\pi RT_0)^{3/2}} \exp\left(-\frac{\boldsymbol{\xi}^2}{2RT_0}\right).$$

Other notations used above are as follows: $\Omega_g$ is the gas region (or pore region), which is defined by the subtraction of the solid region $\Omega_s$ from the entire gap $\Omega = \{X_1 | -L < X_1 < L\}$, i.e., $\Omega_g = \Omega \backslash \Omega_s$; $\partial\Omega_s$ is the solid surface (or the boundary of $\Omega_s$); and $\boldsymbol{n}$ is the unit normal of $\partial\Omega_s$ pointing toward $\Omega_g$ (see Fig. 1). Since the above system is linear in $f$, the following decomposition of $f$ is possible: $f = f^+ + (p^-/p_0)\Phi$, where $f^+$ is the VDF in the case $p^- = 0$ and $\Phi$ is the VDF in the case $p^+ = 0$ and $p^- = p_0$ ($p_0$ is a reference pressure). Furthermore, since $M_0$ solves the above problem for $p^{\pm} = RT_0$, the relation $f^+ - p^+ M_0/(RT_0) = -(p^+/p_0)\Phi$ holds. Because $M_0$ is even with respect to $\boldsymbol{\xi}$, it does not contribute to the mass flow of $f^+$. As a result,

$$\int \xi_i f^+ d\boldsymbol{\xi} = -(p^+/p_0) \int \xi_i \Phi d\boldsymbol{\xi}.$$

Hence, once $\Phi$ is obtained, the mass flow of the gas for any combination of $p^{\pm}$ is recovered. We thus solely study the problem for $\Phi$ and mainly report the obtained results for the following mass flux:

$$\mathcal{M}[\Phi] \equiv \frac{1}{S(\Gamma^+)} \int_{\Gamma^+} (\rho v_1)[\Phi] dS \left(= \frac{1}{S(\Gamma^-)} \int_{\Gamma^-} (\rho v_1)[\Phi] dS\right), \quad \text{(1a)}$$

$$\rho[\Phi] = \int \Phi d\boldsymbol{\xi}, \quad (\rho v_1)[\Phi] = \int \xi_1 \Phi d\boldsymbol{\xi}. \quad \text{(1b)}$$

In the above set of equations, $\Gamma^{\pm} \equiv \{\boldsymbol{X} | X_1 = \pm L, |X_i| < L (i = 2, 3)\}$ and it should be interpreted that $(\rho v_1)[\Phi] = 0$ on $\{\boldsymbol{X} | \boldsymbol{X} \in \Gamma^{\pm} \cap \partial\Omega_s\}$, where $\rho$ is the gas density, $v_1$ is the $X_1$ component of flow velocity, and $S(\Gamma^{\pm}) = (2L)^2$ is the area of the surface $\Gamma^{\pm}$. Note that the mass fluxes on $\Gamma^{\pm}$ agree with each other because of the mass conservation in the gap and the periodicity in the $X_2$- and the $X_3$-direction.

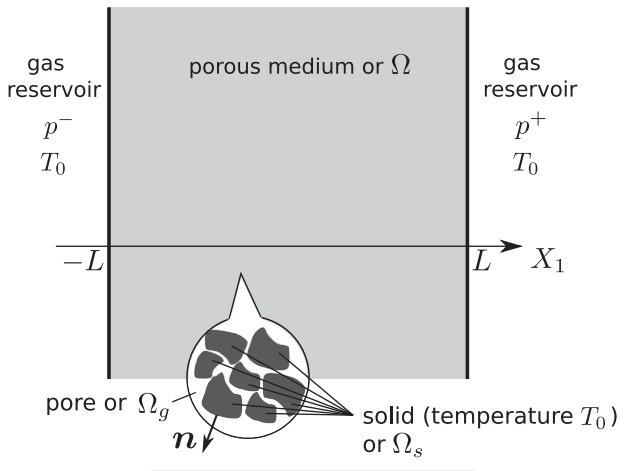


**FIG. 1.** Schematic view of the problem.

### B. Simplified microscopic shape and random configurations

Let us denote by $\widetilde{\Omega}$, $\widetilde{\Omega}_g$, and $\widetilde{\Omega}_s$ the original regions $\Omega$, $\Omega_g$, and $\Omega_s$ restricted in $|X_i| < L (i = 2, 3)$. Obviously, $\widetilde{\Omega}$ is a cube with linear dimension $2L$. Let us divide $\widetilde{\Omega}$ into $(2N)^3$ tiny cubes (or cells) with linear dimension $L/N$ and randomly pick up $N_s$ cells[14] to make them compose the solid region $\widetilde{\Omega}_s$. These $N_s$ cells will be called the solid cells. The remaining $(2N)^3 - N_s$ cells compose the gas region (or

pore) $\widetilde{\Omega}_g$ and will be called the pore cells. The volume fraction of solid $\delta$ is $N_s(2N)^{-3}$, while the volume fraction of the gas region or the porosity $\varepsilon(\equiv 1-\delta)$ is $1-N_s(2N)^{-3}$.

Once the configuration of the solid or $\widetilde{\Omega}_s$ is determined, the boundary-value problem for $\Phi$ is determined to be solved numerically. In the present paper, we have carried out stochastic particle simulations to obtain $\Phi$. The simulations follow the same procedure as the standard direct simulation Monte Carlo (DSMC) method[15] without intermolecular collisions.

The descriptions and computations in the present work are, in principle, to be for spatially three-dimensional cases (to be denoted by $D = 3$), but some results and related discussions are extended to include spatially two-dimensional cases (to be denoted by $D = 2$), aiming at a closer observation of the features of gas transport and a broader assessment of the homogeneous-scatterer model to be proposed in Sec. IV.

## III. SPS RESULTS

Computations for $D = 3$ have been carried out for $N = 8$, 12, 16, and 32 by starting from the reference resting equilibrium state commonly with 1 638 400 test particles. After the steady state is judged to be established, time averaging has been performed to reduce the stochastic fluctuation. The time step is typically $0.005L(2RT_0)^{-1/2}$, and the time average is taken over $10^6$ time steps. The results are summarized mainly in view of the dependence of $\mathcal{M}[\Phi]$ on $\delta$. Figure 2(a) shows a part of the results. Additional computations for two-dimensional cases ($D = 2$) with $N = 16$, 64, 128, and 256 are carried out. A part of the results are shown in Fig. 2(b) for a closer observation of the grain-size impact on the gas transport.[16]

It is observed in Fig. 2(a) that when $\delta$ is relatively small, the mass flux $\mathcal{M}[\Phi]$ decreases rather moderately in the logarithmic scale as $\delta$ increases (phase I). However, as $\delta$ further increases, it tends to decrease abruptly (phase II) and reaches the no conduction state (phase III) beyond a certain critical value of $\delta$. It should be noted that the critical value for the transition from phase II to III tends to be independent of the solid-cell configurations as $N$ is increased. This remarkable feature will be discussed later in Sec. IV B 3. The same tendency from phase I to III is observed as well in the two-dimensional case, though phase II is less clear and the critical value between phases II and III suffers large fluctuations when the grain size is not small enough (see the case $N = 16$). It is also observed in Fig. 2 that besides the porosity or $\delta$, the grain size itself affects the gas transport largely.

Typical flow fields in phases I and II for $D = 3$ are shown in Figs. 3(a)–3(b). Two-dimensional cases (phases I–III) are also shown in Figs. 3(c)–3(e) for a clearer visualization. In the latter, the filled cells show the solid part $\widetilde{\Omega}_s$, and the open and the half-tone cells show the pore part $\widetilde{\Omega}_g$. To be more precise, the open cells indicate the so-called *backbone*, while the half-tone cells indicate the so-called *dead ends*. Here, an *infinite cluster* being a pore region that extends from $X_1 = -L$ to $X_1 = L$, the dead ends are the pore cells connected to the infinite cluster at most at one face,[17] while the backbone is the remaining after pruning the dead ends from the infinite cluster.[9] As is clearly shown in Fig. 3, the gas transport takes place in almost the entire region in phase I [(a) and (c)], while it takes place only in limited subregions of the backbone in phase II [(b) and (d)]. In phase III, there is no longer backbone [(e)], and consequently, no gas transport occurs.

## IV. DISCUSSIONS

### A. A kinetic model with homogeneous scatterer

Besides the usual formulation by the kinetic theory as in Sec. II A, we introduce a kinetic model that treats the gas–solid interaction as a relaxation-type collision integral,

$$\frac{\partial f}{\partial t} + \xi_i \frac{\partial f}{\partial X_i} = A_c(\rho[f]M_0 - f),$$

where $t$ is the time and $A_c$ is a positive constant representing the collision frequency of a gas molecule to the solid. This is a model such that the solid is uniformly embedded in the considered region that the gas molecules occupy and there is no subregion that the molecules are forbidden to enter. The model is motivated from the classical kinetic model for electron transport[18] and will be called the homogeneous-scatterer model (HSM) in the present paper. It may

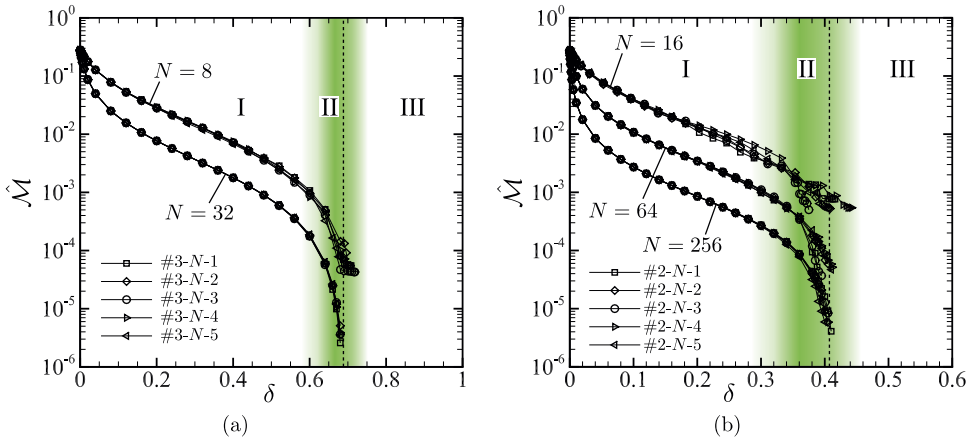


**FIG. 2.** Logarithmic plots of the dimensionless mass flux $\hat{\mathcal{M}} = \mathcal{M}[\Phi]/\{\rho_0(2RT_0)^{1/2}\}$ vs $\delta$ obtained by the SPS, where $\rho_0 = p_0/(RT_0)$: (a) the three-dimensional case with $N = 8$ and 32 and (b) the two-dimensional case with $N = 16$, 64, and 256. The solid cell configuration is determined randomly by a pseudo-random number (PRN) generator. The tag number of the PRN is indicated in the legend. The vertical dashed line indicates the theoretical prediction of the threshold between phases II and III, which is to be discussed in Sec. IV B 3.

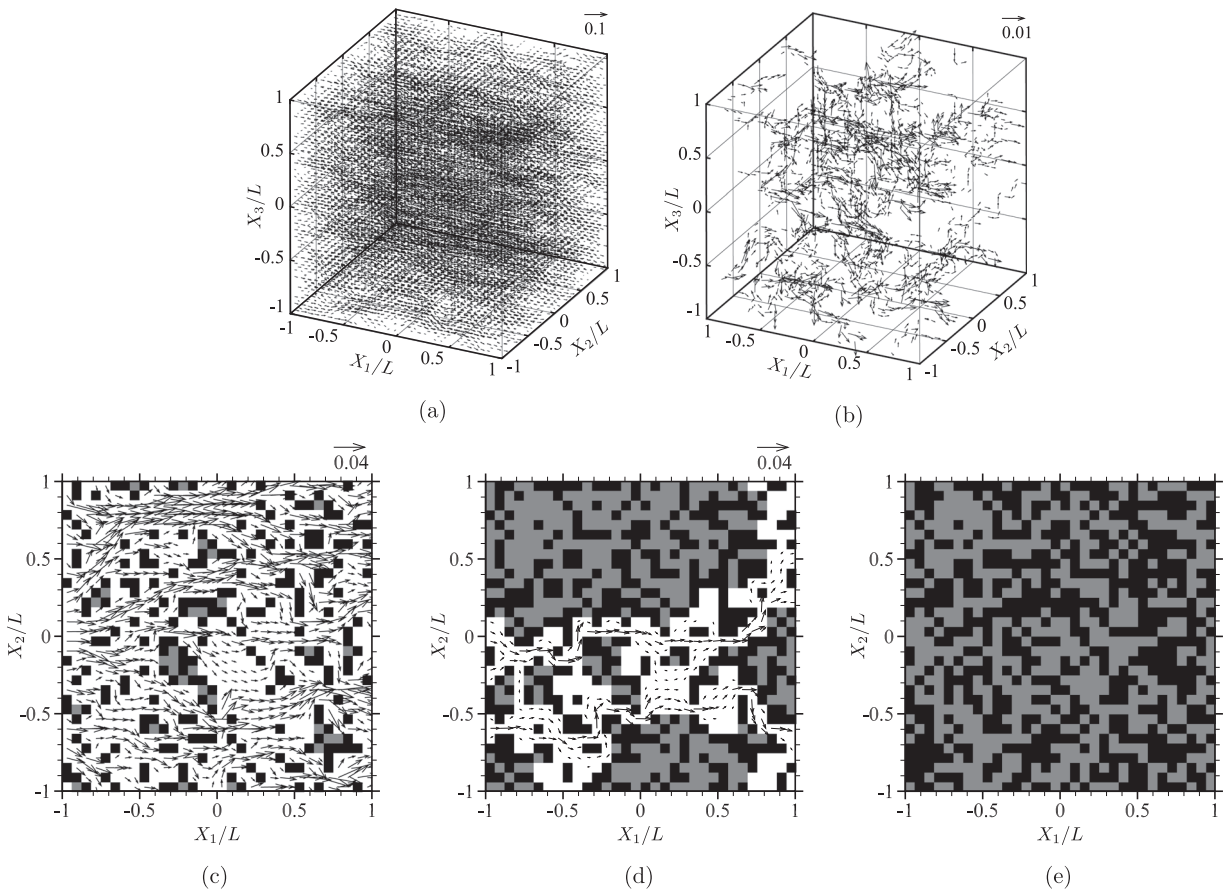


**FIG. 3**. Typical fields of the mass flow $\rho\boldsymbol{v}$ in phases I–III obtained by the SPS. (a) $\delta$ = 0.2802 (phase I), (b) $\delta$ = 0.6406 (phase II), (c) $\delta$ = 0.2031 (phase I), (d) $\delta$ = 0.375 (phase II), and (e) $\delta$ = 0.5 (phase III). (a) and (b) are the three-dimensional cases for $N$ = 16 and PRN sequence No. 3-16-3, while (c)–(e) are the two-dimensional cases for $N$ = 16 and PRN sequence No. 2-16-2. The arrow at the top-right corner of each panel indicates the scale of $\rho\boldsymbol{v}/\{\rho_0(2RT_0)^{1/2}\}$, where $\rho_0 = p_0/(RT_0)$. The mass flow vectors less than the 10% of the maximum are not shown. In (c)–(e), the open, the half-tone, and the filled cell indicate the backbone, the dead end, and the solid cell, respectively.

also be regarded as the simplest version of the detailed approach in Ref. 3. Then, seeking $\Phi$ in Sec. II A in terms of the HSM is reduced to solving the following spatially one-dimensional boundary-value problem for $\Phi$:[19]

$$\xi_1\frac{\partial\Phi}{\partial X_1} = A_c(\rho[\Phi]M_0 - \Phi), \quad X_1 \in \Omega, \tag{2a}$$

$$\Phi|_{X_1=-L} = \frac{p_0}{(2\pi)^{3/2}(RT_0)^{5/2}}\exp\left(-\frac{\boldsymbol{\xi}^2}{2RT_0}\right), \ \xi_1 > 0, \tag{2b}$$

$$\Phi|_{X_1=L} = 0, \quad \xi_1 < 0. \tag{2c}$$

Accordingly, $\mathcal{M}[\Phi]$ is reduced to $(\rho v_1)[\Phi]$,

$$\mathcal{M}[\Phi] = (\rho v_1)[\Phi] = \int \xi_1\Phi d\boldsymbol{\xi}. \tag{3}$$

By using new notations $\hat{\Phi} = \Phi(2\pi)^{3/2}(RT_0)^{5/2}/p_0$, $\hat{\rho} = \rho/\rho_0$ with $\rho_0 = p_0/(RT_0)$, $x_1 = X_1/L$, and $\boldsymbol{\zeta} = \boldsymbol{\xi}/(2RT_0)^{1/2}$ for the dimensionless formulation, the problem is rewritten as

$$\zeta_1\frac{\partial\hat{\Phi}}{\partial x_1} = \frac{2}{\sqrt{\pi}}\frac{1}{\mathrm{Kn}}(\hat{\rho}E - \hat{\Phi}), \quad -1 < x_1 < 1, \tag{4a}$$

$$\hat{\Phi}|_{x_1=-1} = E, \quad \zeta_1 > 0, \tag{4b}$$

$$\hat{\Phi}|_{x_1=1} = 0, \quad \zeta_1 < 0, \tag{4c}$$

where

$$E = \pi^{-3/2}\exp(-\boldsymbol{\zeta}^2), \ \mathrm{Kn} = \frac{1}{A_cL}\sqrt{\frac{8RT_0}{\pi}}. \tag{5}$$

In the HSM, the mass flux is solely controlled by the Knudsen number Kn. Moreover, the system (4) can be reduced to the system for the marginal VDF defined by $\int\hat{\Phi}d\zeta_2d\zeta_3$. These features imply a huge

reduction in computational cost. Figure 4 shows the mass flux vs the Knudsen number computed by the standard finite-difference method applied to the system for the marginal VDF. The simplicity of the HSM also makes it easier to perform the asymptotic analyses for large and small Knudsen numbers. The results are as follows:

for $\mathrm{Kn} \gg 1$

$$\mathcal{M}[\Phi] = \rho_0 (2RT_0)^{1/2} \left( \frac{1}{2\sqrt{\pi}} - \frac{1}{\sqrt{\pi}\mathrm{Kn}} + o\left(\frac{1}{\mathrm{Kn}}\right) \right), \tag{6a}$$

for $\mathrm{Kn} \ll 1$

$$\mathcal{M}[\Phi] = \rho_0 (2RT_0)^{1/2} \left( \frac{\sqrt{\pi}}{8}\mathrm{Kn} + o(\mathrm{Kn}) \right). \tag{6b}$$

These results are shown as well in Fig. 4.

The HSM approach is by far less demanding both numerically and analytically; the mass flux of gas transport is readily obtained, once the Knudsen number is known. Thus, it is desired to establish a way of identifying the effective Knudsen number for a given porous medium.

## B. Effective Knudsen number and some concepts from the percolation theory

Consider the procedure of composing the solid region in Sec. II B. The procedure is none other than the cubic-site problem of discrete percolation. Thus, it is strongly suggested that the transport property near the critical point from phase II to III in Sec. III would follow the prediction of the percolation theory. In this subsection, especially in Sec. IV B 3, we shall introduce a specific way to determine the Knudsen number in the HSM with the aid of some concepts from the percolation theory.

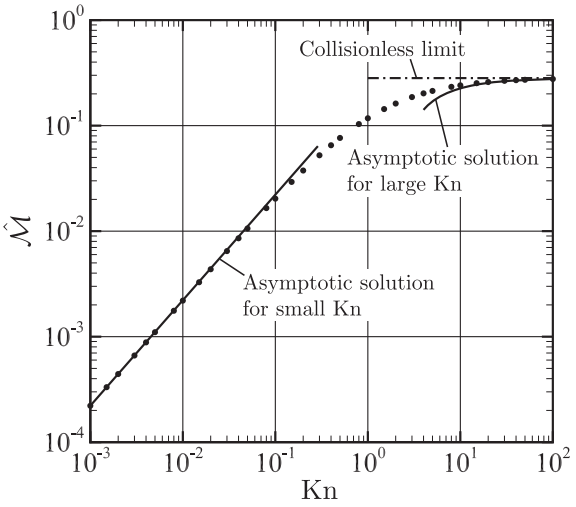


**FIG. 4.** Dimensionless mass flux $\hat{\mathcal{M}} = \mathcal{M}[\Phi]/\{\rho_0(2RT_0)^{1/2}\}$ vs Kn for the HSM. Symbols indicate the numerical results. Solid lines indicate Eqs. (6b) and (6a) without the error term, while the dashed-dotted line indicates the leading term of Eq. (6a).

### 1. Preparation 1: Conductivity for the homogeneous-scatterer model

In order to bridge the HSM to the percolation theory, we need to identify the conductivity for the HSM. To this end, consider the mass flow in the infinite extent of the porous medium induced by a uniform external force.

Suppose that a uniform acceleration $g$ exerts in the $X_1$-direction. Then, the gas behavior is described as follows:

$$\frac{\partial f}{\partial t} + g\frac{\partial f}{\partial \xi_1} = A_c(\rho M_0 - f).$$

Multiplying the above equation with $\xi_1$ and integrating the result over the entire range of $\boldsymbol{\xi}$ yield

$$\frac{\partial \rho v_1}{\partial t} - g\rho = -A_c \rho v_1.$$

In the steady state, the above equation is reduced to

$$A_c \rho v_1 = g\rho.$$

Note that $\rho g$ has the same physical dimension as the pressure gradient. Because of the compressibility of a gas, the mass flow instead of the flow velocity itself is used here to identify the *conductivity* $\sigma$ in the framework of the percolation theory, i.e., $\rho v_1 = -\rho_0 \sigma \times$(imposed pressure gradient). Then, $\sigma$ is found to be inversely proportional to $A_c$,

$$\sigma = \frac{1}{\rho_0 A_c} = \frac{L}{\rho_0}\sqrt{\frac{\pi}{8RT_0}}\mathrm{Kn}. \tag{7}$$

The above relation plays a crucial role in the following discussions because no direct information on Kn occurs in the percolation theory. It is $\sigma$ near the critical point that has been intensively studied and well-understood in the framework of that theory.[7–11]

### 2. Preparation 2: Estimate of the effective Knudsen number for $\varepsilon \simeq 1$ ($\delta \ll 1$)

In this subsection, we consider the problem for $\Phi$ and evaluate the influence of gas–solid collisions on the gas transport near the collisionless limit. Here, the collisionless limit is the case where $\mathrm{Kn} \to \infty$ in the HSM and is the case where there is no solid cell in the usual formulation described in Sec. II. Note that, in the same limit, there are no molecules that travel in the direction opposite to the $X_1$-direction. For later convenience, the two-dimensional case and the three-dimensional case are simultaneously considered, and the spatial dimension is simply denoted by $D$.

In the HSM, the probability of collision per molecule in a small time interval $\Delta t$ is given by $1 - \exp(-A_c \Delta t) \simeq A_c \Delta t$. The molecular velocity after collision is chosen according to the isotropic resting distribution (the resting Maxwellian), so that only half of the molecules change their velocity toward upstream (i.e., the negative $X_1$-direction) to modify the mass flux at $X_1 = -L$ from its collisionless limit. Keeping in mind the above observation, let us consider the corresponding situation under the usual formulation on which the SPS is based. In particular, the case that $\widetilde{\Omega}_s$ is composed of a single solid cell introduced in Sec. II B is the simplest but indeed ideal in discussing the asymptotic behavior near the collisionless limit. Taking into account that no gas molecules travel in the negative $X_1$-direction in that limit, let us estimate the number of molecules

that change the velocity toward upstream after collision with the solid surface. On the upstream face of the solid cell, all the colliding molecules are bounced toward upstream, while on the side faces directed to $\pm X_2$ or $\pm X_3$, only half of the colliding molecules are so because of the diffuse reflection. Because the number of colliding molecules on each side face is a half of that on the surface facing upstream, the total number of molecules bounced toward upstream is estimated as

$$\left(1+\frac{1}{4}\times 2(D-1)\right)\times\mathcal{N}=\frac{D+1}{2}\times\mathcal{N},$$

where $\mathcal{N}$ is the number of molecules colliding with the upstream face of the solid cell and $2(D-1)$ is the number of side faces.[20] Therefore, the total mass of molecules going upstream as a result of collision in the short time interval $\Delta t$ is estimated as

$$\frac{D+1}{2}\frac{1}{2}\rho_0\sqrt{\frac{2RT_0}{\pi}}\Delta t\Delta S,$$

where $\Delta S$ is the area of the upstream face of the solid cell and the mass flux on that face is estimated by the VDF in the collisionless limit. The same quantity is estimated in the HSM as

$$\frac{1}{2}A_c\Delta t\frac{1}{2}\rho_0 V,$$

where $V$ is the volume of $\widetilde{\Omega}$. Equating these, we arrive at

$$A_c=\frac{2}{\sqrt{\pi}}\sqrt{2RT_0}\frac{\Delta S}{V}\frac{D+1}{2}.$$

Note that $V=(2L)^D$ and $\Delta S=(2L/2N)^{D-1}$. Since the case of a single solid cell is considered, $\delta=(1/2N)^D$ and accordingly $\Delta S/V=\delta\times(N/L)$. Substituting these, we obtain

$$A_c=\frac{2}{\sqrt{\pi}}\sqrt{2RT_0}\frac{D+1}{2}\frac{N\delta}{L} \tag{8a}$$

or, equivalently,

$$\mathrm{Kn}\equiv\frac{2}{\sqrt{\pi}}\frac{\sqrt{2RT_0}}{A_cL}=\frac{2}{D+1}\frac{1}{N\delta}. \tag{8b}$$

Here, the parameter $N$ has been retained in order to reflect the solid-grain-size impact on the mass transport property. In what follows, it appears exclusively in the form of $N\delta$.[21] It should be reminded that a single solid-cell arrangement is supposed in the above, and accordingly, no molecules go upstream before colliding with the solid cell. Even when the number of solid cells is small enough, the latter needs to be modified by a fraction $\alpha$ of molecules bounced toward upstream. Then, the factor $(D+1)/2$ given above is to be modified with $1+(1+\alpha)(D-1)/2$. Moreover, as $\delta$ increases, the volume fraction of the solid region becomes no longer negligible. The HSM does not take into account its exclusive effect, which causes the effective Knudsen number to be raised by the factor of the inverse of the volume fraction of the pore region. Accordingly, relation (8b) will be modified as

$$\mathrm{Kn}=\frac{4}{D+1+\alpha(D-1)}\frac{1}{2N\delta(1-\delta)}. \tag{9}$$

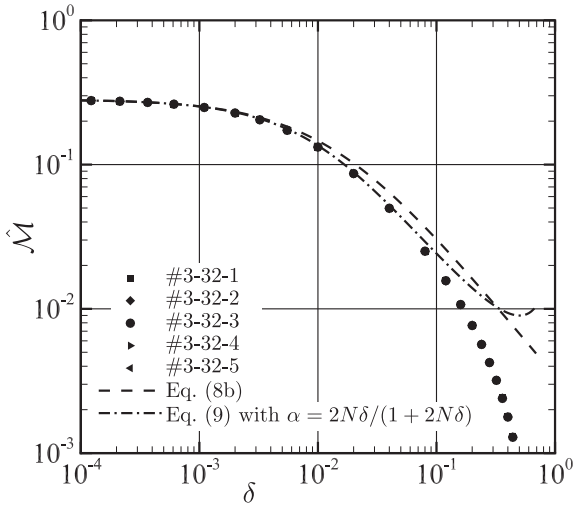


**FIG. 5**. Comparisons of dimensionless mass flux $\hat{\mathcal{M}}=\mathcal{M}[\Phi]/\{\rho_0(2RT_0)^{1/2}\}$ between the SPS and the HSM for $D=3$ and $N=32$. The symbols indicate the SPS, the dashed line indicates the HSM with conversion (8b), and the dashed-dotted line indicates the HSM with Eq. (9) with $\alpha=2N\delta/(1+2N\delta)$. Note that different closed symbols overlap considerably and are hard to be told apart.

Using relations (8b) and (9), the dependence of $\mathcal{M}[\Phi]$ on Kn for the HSM can be converted to that on $\delta$, the result of which is shown in Fig. 5, together with the SPS results (symbols). Obviously, the improvement from Eq. (8b) to Eq. (9), namely, from the dashed to the dashed-dotted line in this figure is limited, even using the following variable $\alpha$:[22]

$$\alpha=\frac{2N\delta}{1+2N\delta}.$$

Further consideration is necessary.

### 3. Some concepts from the percolation theory

The results by the conversion (9) in Sec. IV B 2 are not satisfactory, especially beyond $\delta\simeq 0.1$. It would be due to that the complexity of the backbone in phase II is not taken into account (see Fig. 3). In particular, in approaching the critical point, the fractalness of the infinite cluster of pore cells emerges, and we are motivated to draw some concepts from the percolation theory to reproduce the behavior there.

Here, we show a side evidence for this direction of consideration in Fig. 6. In this figure, $\mathcal{M}[\Phi]$ and the deviation from its free molecular limit are plotted, respectively, against $\delta_c-\delta$ and $\delta$. The slope of the dashed-dotted line in the figure strongly suggests that $\mathcal{M}[\Phi]\propto(\delta_c-\delta)^{\mu}$ for $\delta$ close to $\delta_c$. The origin of exponent $\mu$ and critical number $\delta_c$ will be explained below.

Suppose that the number of pore cells is increased from $\widetilde{\Omega}_s=\widetilde{\Omega}$, although this is opposite to what has been actually done in composing the solid region. According to the percolation theory, the critical point (percolation threshold) appears due to the loss of the characteristic length of the connected pore cells. This, in turn, implies the power-law behavior of the transport property near the critical point.

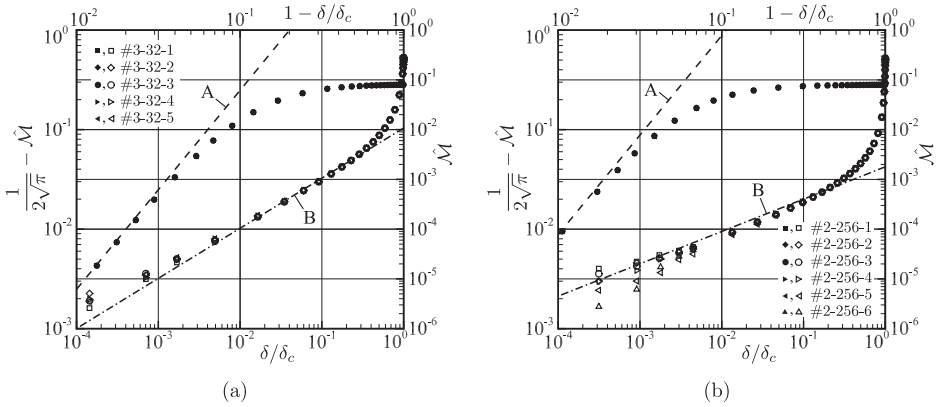


**FIG. 6**. Asymptotic behavior of dimensionless mass flux $\hat{\mathcal{M}} = \mathcal{M}[\Phi]/\{\rho_0(2RT_0)^{1/2}\}$ for small $\delta$ and for small $\delta_c - \delta$. (a) $D = 3$ and $N = 32$ and (b) $D = 2$ and $N = 256$. Closed symbols and line A are plotted against the bottom axis and left axis, while open symbols and line B are plotted against the top axis and right axis, respectively. Both closed and open symbols indicate the SPS results, line A indicates Eq. (6a) with conversion (8b) and line B indicates Eq. (6b) with conversion $\mathrm{Kn} = (1-\delta/\delta_c)^{\mu_D}/[DN\delta_c(1-\delta_c)]$. Note that $\mu_D = 2.0$ and $\delta_c = 0.6884$ in (a), while $\mu_D = 1.3$ and $\delta_c = 0.4073$ in (b).

Moreover, the exponent of the power is known to be independent of the cell geometry, thus called the universal exponent. The universal exponent depends only on the dimension $D$ of the problem, while the critical point may depend on the cell geometry as well as $D$.[23] The exponent $\mu_D$ of the conductivity $\sigma$ is known to obey this rule. In viewing property (7), Kn follows the same universality as $\sigma$, which motivates us to further modify the conversion relation (9) as

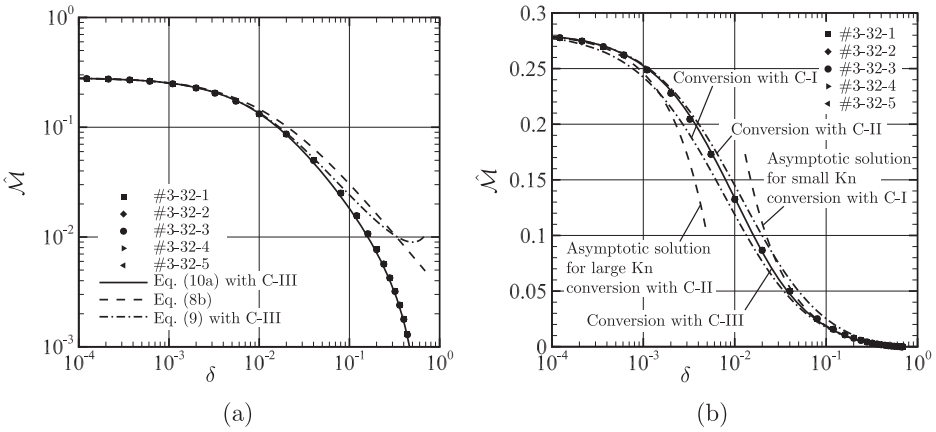


**FIG. 7**. Comparisons of dimensionless mass flux $\hat{\mathcal{M}} = \mathcal{M}[\Phi]/\{\rho_0(2RT_0)^{1/2}\}$ between the HSM and the SPS ($D = 3$ and $N = 32$). Note the difference of the vertical axis scale between (a) and (b). Both in (a) and (b), the symbols indicate the SPS results and the solid line indicates the HSM with the conversion (10a) with C-III. In (a), the dashed-dotted line indicates the HSM with Eq. (9) and C-III (see the caption of Fig. 5), while the dashed line indicates that with conversion (8b). In (b), dashed-dotted lines indicate those with Eq. (10a) for $\alpha = 1$ (C-I) and 0 (C-II), while dashed lines indicate Eq. (6a) with conversion (10a) for $\alpha = 0$ (C-II) and Eq. (6b) with conversion (10a) for $\alpha = 1$ (C-I).

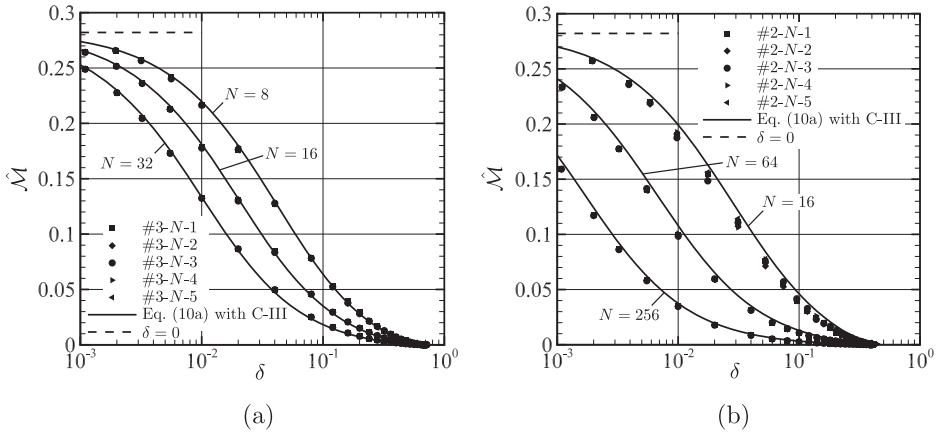


**FIG. 8**. Conversion relation (10a) with C-III and its capability of reproducing the transport property. (a) $D = 3$ and $N = 8$, 16, and 32; (b) $D = 2$ and $N = 16$, 64, and 256. Solid lines indicate the HSM results with conversion (10a) and C-III, while symbols indicate the SPS results. The dashed line indicates the dimensionless mass flux $\hat{\mathcal{M}}$ in the limit $\delta \to 0$.

$$\mathrm{Kn} = \frac{4}{D+1+\alpha(D-1)} \frac{1}{2N\delta(1-\delta)} \left( \frac{\delta_c - \delta}{\delta_c} \right)^{\mu_D}, \tag{10a}$$

$$\alpha = 1 \quad \text{(C-I)}, \tag{10b}$$

$$\alpha = 0 \quad \text{(C-II)}, \tag{10c}$$

$$\alpha = \frac{2N\delta}{1+2N\delta} \quad \text{(C-III)}, \tag{10d}$$

where $D = 2$ or 3, $\delta < \delta_c$, $\delta_c$ is the value of the critical point, and $\mu_D$ is the universal exponent for the conductivity. Because composing the solid region is nothing else than the cubic-site percolation problem in the present work, proper values of $\delta_c$ and $\mu_D$ can be found in the literature. Remind that a pore cell plays the same role as a cubic site in the conductivity problem. The proper values are, thus, $\delta_c = 1-0.3116 = 0.6884$ and $\mu_D = 2.0$ for $D = 3$ ($\delta_c = 1-0.5927 = 0.4073$ and $\mu_D = 1.3$ for $D = 2$).[9] With the new conversion (10a), comparisons are made between the HSM and SPS results in Fig. 7. As is clearly seen, the conversion drastically improves their agreement for any choice of $\alpha$ among Eqs. (10b)–(10d). The best fit is achieved by C-III, namely, Eq. (10a) with Eq. (10d).

Further comparisons are made in Fig. 8, where C-III again achieves good agreement, irrespective of the problem dimension as well as the roughness (grain-size) parameter $N$.

These results support a feasibility of the efficient prediction of gas transport in a porous medium by the simple HSM with the aid of the percolation theory, such as the conversion (10a).

## V. CONCLUSION

In the present paper, we have investigated the transport property of the Knudsen gas in a porous medium. The porous medium is expressed by a collection of small cubic (or square when $D = 2$) solid and pore cells, and over the surface of solid cells, the gas molecules are diffusely reflected. First, stochastic particle simulations have been carried out to identify the conductivity of the Knudsen gas in the medium. Then, a kinetic model with a homogeneous scatterer is introduced, with a special interest in reproducing the gas transport in those simulations. The model has a simple property that the Knudsen number is proportional to the mass flow conductivity and thus allows the use of the accumulated knowledge of the percolation theory. Consequently, by studying the reduced problems in the regimes $\mathrm{Kn} \sim \infty$ (or $\delta \sim 0$) and $\mathrm{Kn} \sim 0$ (or $\delta \sim \delta_c$), an appropriate way of determining the effective Knudsen number for the homogeneous-scatterer model has been identified. It means that a great reduction in computational cost is feasible in predicting the mass flow conductivity of a given porous material because detailed information on micro-structures such as the solid face location/direction and the molecular reflection is not required in that model.

## ACKNOWLEDGMENTS

The present work was supported, in part, by the JSPS KAKENHI (Grant Nos. 15K13870 and 17K18840) and by the Japan-France Integrated Action Program (SAKURA) (Grant No. JPJSBP120193219).

## APPENDIX: SURFACE-TO-VOLUME RATIO AND $N$

The estimate of the grain-size parameter $N$ occurring in (10a) is not obvious in practical applications. However, once the surface-to-volume ratio $\mathcal{S}$ is known (e.g., by the tomography analysis as in Ref. 5), there is a chance, which is explained below. In this appendix, a spatially three-dimensional case is supposed.

In the division of the region into cubic cells, the solid and the pore cell are geometrically identical. Hence, the solid surface area is symmetric with respect to $\delta = 0.5$ as a function of $\delta$, as shown in Fig. 9. More precisely, it is numerically confirmed that the surface-to-volume ratio $\mathcal{S}$ is proportional to $\delta(1-\delta)$, i.e., $\mathcal{S} = C\delta(1-\delta)$ ($C$: constant). Now, let us estimate $C$ by a simple consideration in the regime of $\delta \sim 0$. In that regime, the solid cells are sparsely distributed and are rarely in contact with each other. Hence, $\mathcal{S}$ is well estimated

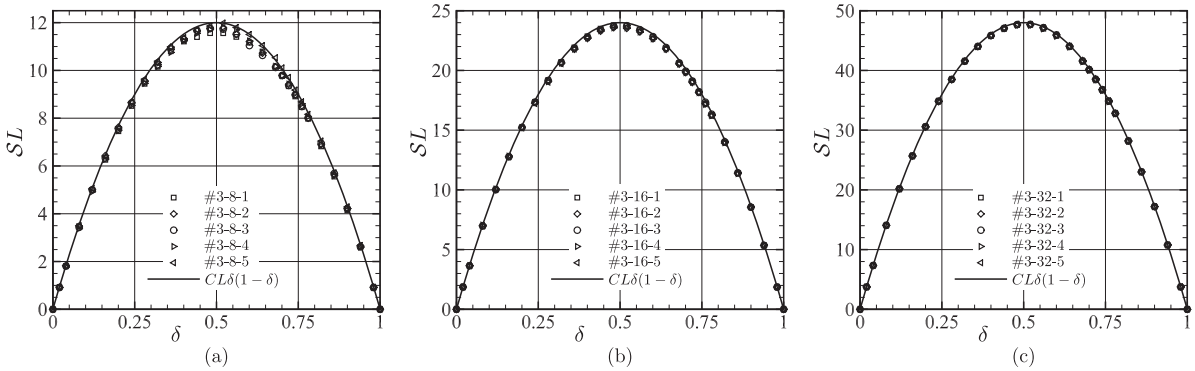


**FIG. 9**. Dependence of the surface-to-volume ratio on $\delta$. (a) $N = 8$, (b) $N = 16$, and (c) $N = 32$. Symbols indicate the numerical results. The tag number of the PRN is indicated in the legend. The solid line indicates the theoretical consequence $\mathcal{S} = C\delta(1-\delta)$, where $C = 6N/L$.

as

$$\mathcal{S} = 6\left(\frac{L}{N}\right)^2 \frac{N_s}{(2L)^3} = 6\left(\frac{L}{N}\right)^2 \frac{(2N)^3\delta}{(2L)^3} = 6(N/L)\delta. \quad \text{(A1)}$$

Neglecting $\delta^2$ term in $\mathcal{S} = C\delta(1-\delta)$ and comparing with (A1), $C$ is estimated as $C = 6(N/L)$, which, in turn, leads to the following estimate of $N$ in terms of $\mathcal{S}$ and $\delta$:

$$N = \frac{L}{6}\frac{\mathcal{S}}{\delta(1-\delta)} = \frac{V^{1/3}}{12}\frac{\mathcal{S}}{\delta(1-\delta)}, \quad \text{(A2)}$$

where $V$ is the volume of the region, i.e., $V = (2L)^3$.

## DATA AVAILABILITY

The data that support the findings of this study are available from the corresponding author upon reasonable request.

## REFERENCES


[1] S. Nakaye and H. Sugimoto, "Demonstration of a gas separator composed of Knudsen pumps," Vacuum **125**, 154–164 (2016).

[2] L. Wu, M. T. Ho, L. Germanou, X.-J. Gu, C. Liu, K. Xu, and Y. Zhang, "On the apparent permeability of porous media in rarefied gas flows," J. Fluid Mech. **822**, 398–417 (2017).

[3] V. Pavan and L. Oxarango, "A new momentum equation for gas flow in porous media: The Klinkenberg effect seen through the kinetic theory," J. Stat. Phys. **126**, 355–389 (2007).

[4] Y. Kawagoe, T. Oshima, K. Tomarikawa, T. Tokumasu, T. Koido, and S. Yonemura, "A study on pressure-driven gas transport in porous media: From nanoscale to microscale," Microfluid. Nanofluid. **20**, 162 (2016).

[5] M. V. Johansson, F. Testa, P. Perrier, J. Vicente, J. P. Bonnet, P. Moulin, and I. Graur, "Determination of an effective pore dimension for microporous media," Int. J. Heat Mass Transfer **142**, 118412 (2019).

[6] C. Savaro, J. P. Bonnet, M. V. Johansson, P. Perrier, I. Graur, and P. Moulin, "Gas permeability in rarefied flow conditions for characterization of mineral membrane support," Eur. J. Mech.: B/Fluids **79**, 44–53 (2020).

[7] T. Odagaki, *Introduction to Percolation Physics*, 5th ed. (Shokabo, Tokyo, 2002) (in Japanese).

[8] D. Stauffer and A. Aharony, *Introduction to Percolation Theory*, Revised 2nd ed. (Taylor & Francis, London, 1994).

[9] A. Hunt, R. Ewing, and B. Ghanbarian, *Percolation Theory for Flow in Porous Media*, 3rd ed. (Springer, Cham, 2014).

[10] H. Scher and R. Zallen, "Critical density in percolation processes," J. Chem. Phys. **53**, 3759–3761 (1970).

[11] V. K. S. Shante and S. Kirkpatrick, "An introduction to percolation theory," Adv. Phys. **20**, 325–357 (1971).

[12] Y. Sone, *Molecular Gas Dynamics* (Birkhäuser, Boston, 2007), Supplementary Notes and Errata is available from Kyoto University Research Information Repository, http://hdl.handle.net/2433/66098.

[13] C. Cercignani, *The Boltzmann Equation and Its Applications* (Springer, New York, 1988).

[14] The random choice is made with equal probability, supposing that the porous medium is spatially homogeneous.

[15] G. A. Bird, *Molecular Gas Dynamics and the Direct Simulation of Gas Flows* (Oxford University Press, New York, 1994).

[16] Here, the two-dimensional condition applies only to the physical space, and the molecular velocity space remains three-dimensional. In this context, $\widetilde{\Omega}$ is a square region, which is divided into $(2N)^2$ tiny square cells with linear dimension $L/N$. Then, $N_s$ cells are randomly picked up to compose the solid part. Hence, $\delta = N_s(2N)^{-2}$, $\varepsilon = 1 - N_s(2N)^{-2}$, and the area $S(\Gamma^{\pm})$ in Eq. (1a) is given by $S(\Gamma^{\pm}) = 2L$.

[17] In Ref. 9, the *dead end* is defined by a pore cell that is connected to the infinite cluster only at one face. In the present definition, a pore cell whose sides are all in contact with the solid is also categorized as a dead end [see the half-tone cells in Fig. 3(e)].

[18] C. Kittel, *Introduction to Solid State Physics*, 8th ed. (John Wiley & Sons, New York, 2005), Appendix F.

[19] Rigorously speaking, a different notation should be used for the present $\Phi$ because the mathematical problem is different from that in Sec. II A. However, for the clarity of correspondence, we dare to use the same notation. The same comment applies to $\mathcal{M}[\Phi]$, etc.

[20] Due to the periodic condition in the $X_2$- and the $X_3$-direction, a part of molecules may collide multiple times with the solid cell. However, their effect is of higher order and is neglected here.

[21] Because the number of solid cells is $(2N)^D\delta$ and the cross section of each cell is $(L/N)^{D-1}$, the collision frequency is proportional to $N\delta$ in a straightforward interpretation. Hence, it is natural to have the present relation that $\mathrm{Kn} \propto 1/(N\delta)$.

[22] As the first approximation for small $\delta$, the effect of bounced upstream can be neglected, leading to $\alpha = 0$. As far as the number of solid cells is small, the approximation can be improved by taking into account the fraction of their projection onto the $X_2X_3$-plane, which is estimated as $2N\delta$, the number of cells $(2N)^D\delta$ divided by $(2N)^{D-1}$. Hence, $\alpha \sim 2N\delta$ for $N\delta \ll 1$. In the meantime, $\alpha$ is expected to approach unity as $\delta$ is increased. No more *a priori* information seems to be available about $\alpha$, except for its monotonicity in $\delta$. The present choice of variable $\alpha$ is among the simplest realizations of those properties.

[23] As for the critical point, some semi-empirical universalities can be found in the literature. For instance, the critical volume fraction $V_c \equiv fp_c$, which is introduced in Ref. 10 as the critical percolation density, is found to be around 0.154 [or scarcely different from 0.17 according to Ref. 9 (Sec. 1.21)] for three-dimensional regular-lattice cases, where $f$ is the filling factor (should not be confused with the VDF) and $p_c$ the critical probability. The former is 0.5236 (cubic site) and the latter $1 - \delta_c$.